The CUE1 domain of the SNF2-like chromatin remodeler SMARCAD1 mediates its association with KRAB-associated protein 1 (KAP1) and KAP1 target genes

Received for publication, November 16, 2017, and in revised form, December 13, 2017 Published, Papers in Press, December 28, 2017, DOI 10.1074/jbc.RA117.000959

Dong Ding[‡1], Philipp Bergmaier[‡1], Parysatis Sachs[‡], Marius Klangwart[‡], Tamina Rückert[‡], Nora Bartels[‡], Jeroen Demmers[§], Mike Dekker[¶], Raymond A. Poot[¶], and Jacqueline E. Mermoud[‡2]

From the [‡]Institute of Molecular Biology and Tumour Research, Philipps University Marburg, Marburg 35043, Germany and the [§]Center for Proteomics and [¶]Department of Cell Biology, Erasmus Medical Center, 3015 CN Rotterdam, The Netherlands

Edited by Ronald C. Wek

Chromatin in embryonic stem cells (ESCs) differs markedly from that in somatic cells, with ESCs exhibiting a more open chromatin configuration. Accordingly, ATP-dependent chromatin remodeling complexes are important regulators of ESC homeostasis. Depletion of the remodeler SMARCAD1, an ATPase of the SNF2 family, has been shown to affect stem cell state, but the mechanistic explanation for this effect is unknown. Here, we set out to gain further insights into the function of SMARCAD1 in mouse ESCs. We identified KRAB-associated protein 1 (KAP1) as the stoichiometric binding partner of SMARCAD1 in ESCs. We found that this interaction occurs on chromatin and that SMARCAD1 binds to different classes of KAP1 target genes, including zinc finger protein (ZFP) and imprinted genes. We also found that the RING B-box coiled-coil (RBCC) domain in KAP1 and the proximal coupling of ubiquitin conjugation to ER degradation (CUE) domain in SMARCAD1 mediate their direct interaction. Of note, retention of SMARCAD1 in the nucleus depended on KAP1 in both mouse ESCs and human somatic cells. Mutations in the CUE1 domain of SMARCAD1 perturbed the binding to KAP1 *in vitro* and *in vivo*. Accordingly, an intact CUE1 domain was required for tethering this remodeler to the nucleus. Moreover, mutation of the CUE1 domain compromised SMARCAD1 binding to KAP1 target genes. Taken together, our results reveal a mechanism that localizes SMARCAD1 to genomic sites through the interaction of SMARCAD1's CUE1 motif with KAP1.

Embryonic stem cells (ESCs)[3] are pluripotent and thus able to respond to inductive signals leading to differentiation into every cell type of the body while simultaneously balancing the ability to undergo self-renewal in each replication cycle. Apart from transcription factors, the importance of ATP-dependent chromatin remodeling enzymes for supporting and reinforcing stem cell homeostasis is increasingly recognized (1–7). ATP-dependent chromatin remodeling enzymes modulate interactions between DNA and histones, driving changes in nucleosome position, structure, or composition, thereby regulating the access of other proteins, such as transcription factors or chromatin modifiers. As a result, these enzymes are central to the control of chromatin structure and genome function. Interfering with their normal expression frequently results in impairment of embryonic development and pluripotency (1, 2, 8). For instance, brahma-associated factor (BAF) is an example of a remodeling complex that directly interacts with components of the pluripotency network to regulate the expression of ESC regulators (1, 2, 5). More recently, knockdown of *Smarcad1* (SWI/SNF-related, matrix-associated actin-dependent regulator of chromatin, subfamily A, containing DEAD/H box 1) was recognized to elicit a change in the pluripotent state (9–11).

The SMARCAD1 family of remodelers belongs to the evolutionarily most conserved remodeling complexes and includes Fun30 in *Saccharomyces cerevisiae*, Fft3 in *Schizosaccharomyces pombe*, and SMARCAD1/Etl1 in mammals. One conclusion from studies of the individual family members is that they are important for the regulation and maintenance of functional chromatin domains (12–19). Depletion of this enzyme results in an open chromatin conformation in normally transcriptionally repressed regions and can affect gene expression, suggesting that SMARCAD1 ensures correct chromatin structure of silent domains. SMARCAD1 can also activate transcription together with co-activator p300/CBP (CREB-binding protein), and interactions with the transcription machinery have recently been reported in *S. pombe* (20, 21). In addition, SMARCAD1 is involved in double-strand break repair (22). Biochemically, this remodeler has been best characterized in budding yeast. Fun30 is capable of binding chromatin and DNA *in vitro* with a preference for single-stranded chromatin and exhibits activity in ATP-dependent chromatin remodeling assays (19, 23, 24). A homozygous mutation of this remodeler in the mouse results in growth retardation, prenatal and perinatal lethality, reduced fertility, and skeletal abnormali-

This work was supported by a grant from the Deutsche Forschungsgemeinschaft (TRR81 to J. M., P. S., and P. B.). The authors declare that they have no conflicts of interest with the contents of this article.

This article contains Table S1 and Figs. S1–S6.

[1] Both authors contributed equally to this work.

[2] To whom correspondence should be addressed. Tel.: 49-6421-282-6349; E-mail: mermoud@imt.uni-marburg.de.

[3] The abbreviations used are: ESC, embryonic stem cell; emPAI, exponentially modified protein abundance index; RBCC, RING B-box coiled-coil; PB, plant homeodomain and bromodomain; DAPI, 4′,6-diamidino-2-phenylindole; qPCR, quantitative PCR; H3K9, histone H3 Lys-9; H3K9me3, H3K9 trimethylation; KD, knockdown; esiRNA, endoribonuclease-prepared siRNA; PMSF, phenylmethylsulfonyl fluoride; PCV, packed cell volume; GST, glutathione S-transferase; aa, amino acids; BAF, brahma-associated factor; CREB, cAMP-response element–binding protein.

ties (25). Whereas SMARCAD1 is expressed throughout development, its function is best characterized in adult cells, yet SMARCAD1 levels are particularly high in the inner cell mass of the blastocyst embryo and in ESCs (26–28). ESCs depleted for SMARCAD1 lose the typical morphology and show defects in exit from self-renewal (9–11). Despite its importance in ESCs, little is known about SMARCAD1 function and regulation in the context of the chromatin environment in pluripotent cells.

SWI/SNF proteins typically function together with accessory proteins that help to direct these enzymes to specific genomic loci, modulate their activity, and integrate chromatin remodeling with distinct cellular pathways. Besides, changes in the composition and stoichiometry of these complexes during mammalian development confer unique roles to remodelers (2, 8, 29). For instance, specialized assemblies of the BAF remodeling complex with cell type–specific subunits were found to be critical for progression from pluripotency to multipotency to committed neurons. We and others have previously identified candidate accessory factors of SMARCAD1 in human somatic cells (13, 30). Prominent among them was the KRAB-associated protein 1, KAP1 (TRIM28; TIF1β). Conversely, KAP1 purifications from HEK293 contain SMARCAD1 (31). KAP1 is an important regulator of normal development and differentiation. It has transcriptional and non-transcriptional roles and, like SMARCAD1, is involved in DNA repair and chromatin replication (13, 32–35). How KAP1 functions in the context of the human SMARCAD1 remodeling complex is not known. Open questions also concern whether KAP1 is a tissue-specific or constitutive interaction partner of SMARCAD1.

In this study, we present evidence for a physical and regulatory link between SMARCAD1 and KAP1 in mouse ESCs. Our results reveal that KAP1 target genes are bound by SMARCAD1, and we provide mechanistic insights into how they are recognized.

Results

KAP1 is a stoichiometric component of SMARCAD1 mouse ESC complexes

To identify the major functional component(s) of SMARCAD1 remodeling complexes in pluripotent cells, we generated mouse ESCs stably expressing FLAG-tagged SMARCAD1 protein (Fig. S1*A*) to utilize in an unbiased purification coupled to a proteomic analysis. Tagged SMARCAD1 was nuclear and localized indistinguishably from the endogenous protein (Fig. S1*B*). FLAG affinity purification was carried out under conditions where nucleic acids were degraded to rule out protein-protein interactions bridged by DNA/RNA (Fig. S1, *C* and *D*). Silver stain of proteins purified from FLAG-SMARCAD1 nuclear extracts identified two major protein bands not present in purifications from control extracts; the protein migrating at about 130 kDa corresponds to tagged SMARCAD1 (Fig. 1*A*). The protein at 100 kDa was identified by mass spectrometry analysis as KAP1 in three independent purification experiments (Fig. 1*B*). We applied the exponentially modified protein abundance index (emPAI; (36)) to the proteomic data sets. SMARCAD1 and KAP1 have comparable emPAI scores, indicating that both proteins are of similar abundance and thus stoichiometric in the FLAG purification (Fig. 1*B*). Next, we sought to confirm this association with endogenous proteins. Soluble and chromatin fractions were prepared from ES cellular extracts to further localize SMARCAD1 and KAP1 (Fig. 1*C*). Endogenous proteins co-eluted and were found predominantly in the soluble fraction. About 20% of the total pool of SMARCAD1 and KAP1 was found to be in the chromatin fraction in an asynchronous ESC population. A SMARCAD1 antibody efficiently co-immunoprecipitated KAP1 from ESC extracts (Fig. 1*D*). Collectively, these data show that SMARCAD1 forms a stable complex with KAP1 in mouse ESCs. This extends previous observations made in human somatic cell lines (13, 30) and indicates that the association between SMARCAD1 and KAP1 is conserved in multiple cell lines, human and mouse, of different developmental stages, pluripotent and differentiated.

The RBCC domain of KAP1 is required for SMARCAD1 interaction

KAP1 is a modular protein and harbors several functional domains (Fig. 2*A* (34, 35)). The RING B-box coiled-coil (RBCC) domain has been characterized as a protein interaction interface and binds KRAB-ZNF proteins involved in KAP1 recruitment to the genome. A centrally located motif recognized by the heterochromatin protein HP1 and the C-terminal part of KAP1 fulfill silencing functions. To establish which domain of KAP1 mediates the interaction with SMARCAD1, glutathione *S*-transferase (GST) pull-down experiments were performed with a series of recombinant GST-KAP1 deletion mutants (Fig. 2, *A* and *B*). SMARCAD1 bound to GST–full-length KAP1 but not to GST (Fig. 2*B*, compare *lanes 1* and *7*). Deletion of the C-terminal plant homeodomain and bromodomain (PB), which has been previously shown to recruit the chromatin remodeler CHD3 and the histone methyltransferase SETDB1 (34, 35), did not abolish the interaction with SMARCAD1 (Fig. 2*B*, *lane 2*). However, binding was abolished when the N-terminal RBCC domain was absent (Fig. 2*B*, *lane 3*). Notably, the 376-amino acid RBCC domain alone can mediate the interaction with SMARCAD1 (Fig. 2*B*, *lane 4*). Neither the HP1 binding domain (*lane 5*) nor the C-terminal part of KAP1 (*lane 6*) bound SMARCAD1. These results show that the RBCC domain of KAP1 is both necessary and sufficient for its interaction with SMARCAD1 *in vitro*.

The CUE1 domain of SMARCAD1 mediates the interaction with KAP1

The signature motif of ATP-dependent chromatin remodeling enzymes is a conserved SNF2-like ATPase domain. In addition, mammalian SMARCAD1 contains tandem copies of a CUE domain located near the N terminus (Fig. 2*C*) (18). CUE domains are predicted ubiquitin-binding motifs stretching over ~40 amino acids (37). We previously found that a recombinant GST-SMARCAD1 double CUE domain construct (amino acids 131–367) robustly associated with KAP1 from HeLa nuclear extracts (13). The double CUE domain is thus a candidate for mediating a direct physical interaction with KAP1. We corrob-

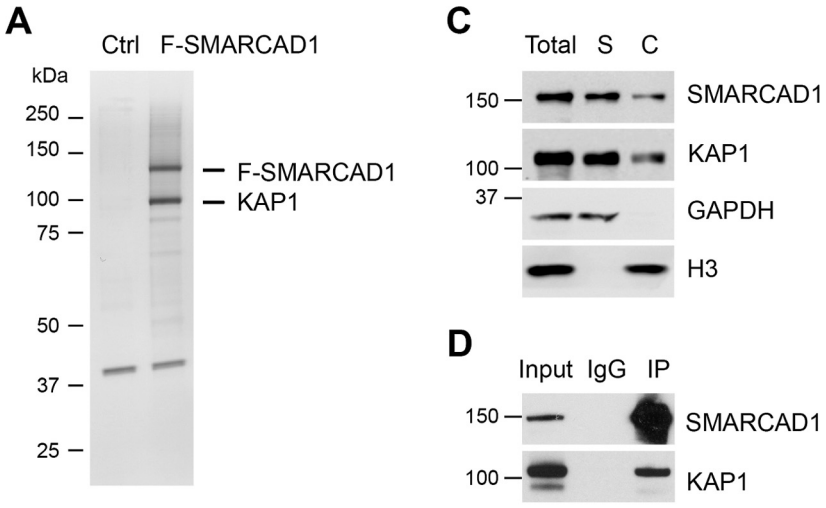

B

Protein (Accession)	1st IP			2nd IP			3rd IP		
	M	P	emPAI	M	P	emPAI	M	P	emPAI
SMARCAD1 (Q04692)	625	17	0.73	2163	42	6.44	3425 (101)	56 (3)	22.61 (0.09)
KAP1 (Q62318)	516 (48)	11 (1)	0.83 (0.04)	1810 (54)	33 (1)	6.58 (0.04)	2297 (181)	40 (5)	16.16 (0.19)

Figure 1. KAP1 (TRIM28) is a major component of SMARCAD1 complexes in mouse ESCs. *A*, silver-stained SDS-polyacrylamide gel of a representative FLAG-SMARCAD1 and control purification from PGK12.1 ESCs. FLAG-SMARCAD1, KAP1, and M_r markers are indicated. *B*, mass spectrometry data from SMARCAD1 affinity purifications. Uniprot accession numbers are given. The Mascot score (*M*), number of identified unique peptides (*P*), and the emPAI from three purifications are shown. The Mascot score is the probability that the observed match is a random event. The emPAI (36) is a semiquantitative analytical value indicating the relative abundance of peptides within the sample. Scores for the corresponding control purification are shown in parentheses. *C*, Western blot analysis of ESCs biochemically fractionated into chromatin-enriched (*C*) and soluble fractions (*S*). Endogenous SMARCAD1 and KAP1 proteins from E14 cells are readily extractable with 0.1% Triton (*S*); ~20% of each protein remains associated with the chromatin (*C*). Controls, GAPDH, and histone H3 separate into the appropriate subfractions. *D*, endogenous SMARCAD1 was immunoprecipitated from J1 ESC extracts in the presence of Benzonase and ethidium bromide. Immunoprecipitates (*IP*) and 5% of the input were separated by SDS-PAGE and KAP1 was detected by immunoblotting as co-immunoprecipitating protein.

orated this in a series of GST pulldown experiments *in vitro* (Fig. 2*C*); full-length GST-SMARCAD1 and GST-double CUE but not GST alone interact with baculovirus-expressed KAP1. Interestingly, the CUE1 domain is sufficient to mediate KAP1 binding, whereas CUE2 is not required (Fig. 2*C*, compare *lanes 4* and *5*). To verify the CUE1 KAP1 interaction, we mutated key residues in the CUE1 domain. CUE domains typically fold into three-helix bundles (Fig. S2) in which two highly conserved sequence motifs are involved in stabilizing the hydrophobic core and in the efficient interaction with ubiquitin (37). These are a dileucine motif in α helix 3 and an N-terminal FP motif (Fig. S2) (37). We converted the invariant proline at position 170 in the FP motif in SMARCAD1 to a glycine. Independently, we replaced Phe-169 and Leu-196, which contribute to the hydrophobic core, with polar amino acids (Fig. S2). Recombinant proteins with these CUE1 mutations were tested for their ability to pull down KAP1. Whereas the P170G exchange had little effect on binding (Fig. 2*C*, *lane 6*) the double mutation targeting the two highly conserved sequence motifs characterizing CUE domains completely abolished the interaction with KAP1 (Fig. 2*C*, *lane 7*). This suggests that preserving a CUE1 protein fold with a hydrophobic core is necessary for stable KAP1 interaction.

The involvement of a CUE domain in the interaction with KAP1 implies that SMARCAD1 may interact with ubiquitylated KAP1. However, posttranslational modification of KAP1 by ubiquitylation is unlikely to be important for the interaction with SMARCAD1 because pure recombinant proteins are able to interact. To investigate this further, we considered whether ubiquitin can compete for the interaction with KAP1 (Fig. 2*D*). We estimated the binding affinity of SMARCAD1 CUE1-KAP1 to be in the micromolar or submicromolar range, as the binding reactions routinely contained low micromolar KAP1 and GST-CUE1 proteins. Pure ubiquitin was titrated into the GST pulldown assays up to a concentration of a 1000-fold molar excess over KAP1 (Fig. 2*D*, *middle*). No detectable competition occurred, demonstrating that the CUE1 domain binds to KAP1 with significantly higher affinity than to ubiquitin (Fig. 2*D*, *top*). In summary, whereas CUE domains are recognized as canonical ubiquitin binding domains, the CUE1 domain in SMARCAD1 displays unusual characteristics in that it recognizes unmodified KAP1.

Steady-state levels of SMARCAD1 depend on KAP1

Our experiments so far showed a direct physical interaction between SMARCAD1 and KAP1. To investigate the interdependence of these proteins, ESCs were depleted for either KAP1 or SMARCAD1 by RNAi, and the protein and RNA levels of the other partner were assessed in immunoblots and by quantitative RT-PCR. Depletion of KAP1 resulted in concomi-

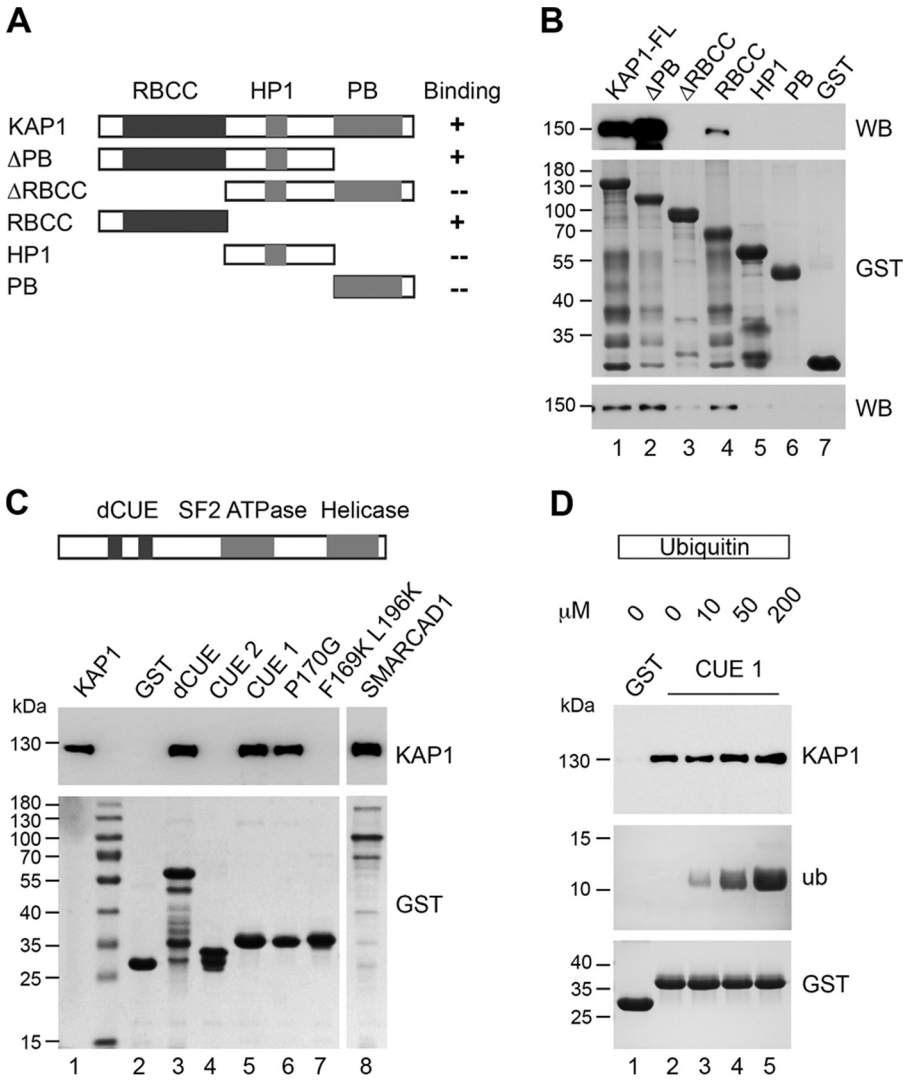

Figure 2. SMARCAD1 and KAP1 interact directly with each other via their RBCC and CUE1 domains. *A* and *B*, the RBCC domain of KAP1 mediates the interaction with SMARCAD1. *A*, GST fusion constructs of KAP1 and deletion mutants. *RBCC*, ring finger, B-box, zinc finger, coiled-coil; *HP1*, heterochromatin protein 1 domain; *PB*, PHD and bromodomain. *B* (*middle*), InstantBlue-stained polyacrylamide gel of purified GST-KAP1 proteins. GST-pulldown assays were performed with *in vitro* transcribed/translated V5-SMARCAD1 (*top panel*) or His-SMARCAD1 expressed in insect cells (*bottom*). Bound proteins were detected by Western blotting with anti-SMARCAD1 or anti-V5 antibody (*WB*). *C*, the CUE1 domain of SMARCAD1 binds to KAP1. GST-pulldown assays were performed with GST fusion proteins as indicated and His-KAP1 expressed in insect cells. Shown is a diagram of full-length GST-SMARCAD1 (amino acids 1–1026); CUE, ATPase, and helicase domains are indicated. *Top*, KAP1 bound to SMARCAD1 and SMARCAD1 domains detected by immunoblotting with anti-KAP1 antibody. KAP1 (*lane 1*) is the input protein loaded at 20% of the amount added to each binding reaction. *Bottom*, GST fusion proteins indicating that comparable amounts were used in each binding reaction. *D*, SMARCAD1 binds KAP1 with higher affinity than ubiquitin. Shown is a competition experiment titrating pure ubiquitin (0, 10, 50, and 200 μM) into GST-pulldown assays containing 1 μM GST-CUE1 and 0.2 μM KAP1. *Top*, bound KAP1 detected by immunoblotting. *Middle* and *bottom*, InstantBlue-stained PAGE gels of ubiquitin (*ub*, *middle*) or GST fusion proteins (*GST*, *bottom*).

tant reduction of SMARCAD1 protein levels without affecting lamin B1 (Fig. 3*A* (*left*), compare *lanes 1* and *2*). This was seen in multiple independent ESC lines (E14, J1, and PGK12.1) with different methods of KAP1 depletion (shRNA or esiRNA) and occurred progressively; cells depleted for longer time periods exhibited lower SMARCAD1 levels than at earlier time points (Fig. 3*A*, 5 days; Fig. S3, 3 days) (data not shown).

The *Smarcad1* gene is bound by the core pluripotency transcription factors NANOG, OCT4, and SOX2, and its expression is down-regulated upon differentiation (26, 27, 38). We therefore considered two possible explanations for reduced SMARCAD1 levels: KAP1 directly affects SMARCAD1 stability in ESCs and/or the reduction is an indirect consequence of cell differentiation. ESCs are known to progressively lose pluripotency upon KAP1 removal (3, 39–41), and consistent with this, we detected reduced levels of the pluripotency protein NANOG following KAP1 depletion (Fig. 3*A* (*left*), compare *lanes 1* and *2*). To test whether the observed drop in SMARCAD1 levels is due to reduced self-renewal capability of KAP1 knockdown cells, we overexpressed epitope-tagged SMARCAD1 driven by a chicken β-actin promoter, which is not regulated by the pluripotency network. When we depleted KAP1 under these conditions, SMARCAD1 levels were also severely diminished (Fig. 3*A* (*left*), compare *lanes 3* and *4*), suggesting that the effect on SMARCAD1 steady-state levels is not solely a direct consequence of differentiation. We also observed that mRNA levels of SMARCAD1 were affected upon KAP1

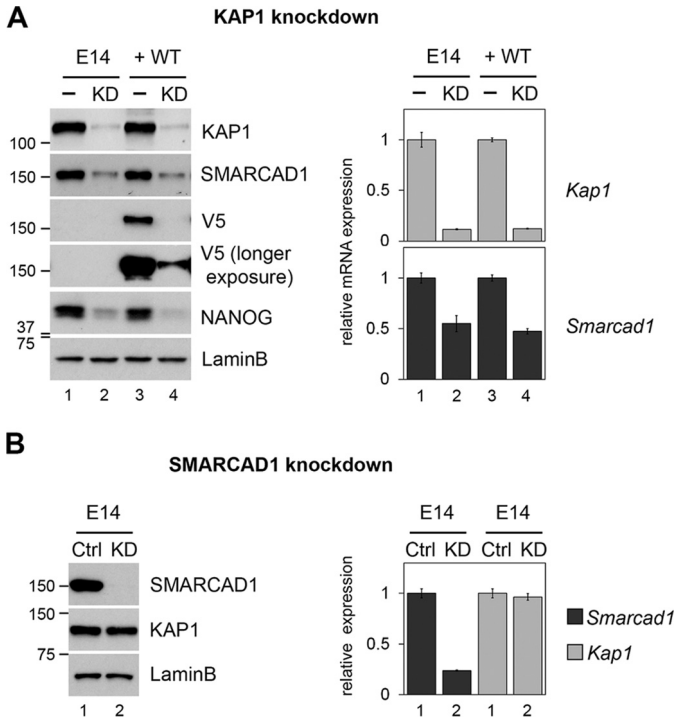

Figure 3. KAP1 depletion affects SMARCAD1 RNA and protein levels in ESCs. *A*, endogenous and exogenously expressed SMARCAD1 levels fall when KAP1 is depleted by 5-day treatment with a specific shRNA (*KD*) compared with untreated ES cells (−). *Left*, immunoblot detection of the levels of endogenous SMARCAD1 (*lanes 1* and *2*) and of V5-tagged SMARCAD1 overexpressed in E14 cells (+ *WT*; *lanes 3* and *4*). KAP1 levels are significantly reduced (*top*), and endogenous SMARCAD1 levels fall (*SMARCAD1 panel*) as do levels of the exogenous protein (*V5 panel*). Lamin B1 is used as a loading control. Pluripotency marker NANOG levels are reduced upon KAP1 depletion. *Right*, quantitative RT-PCR analysis of *Smarcad1* and *Kap1* in the same samples as to the *left*. Gene expression was normalized to the average of three housekeeping genes and is presented as mean ± S.D. (*error bars*) of three technical replicates. *B*, analysis of SMARCAD1, KAP1, and lamin B1 in E14 cells depleted for SMARCAD1. Stable knockdown with an shRNA specific for *Smarcad1* in parallel with a non-targeting shRNA (*Ctrl*) effectively reduced the expression of SMARCAD1 but had no detectable impact on KAP1 protein (*left*) or RNA levels (*right*). Similar results were obtained with a different shRNA and ES cell line (data not shown). Data are presented as mean ± S.E. of three technical replicates.

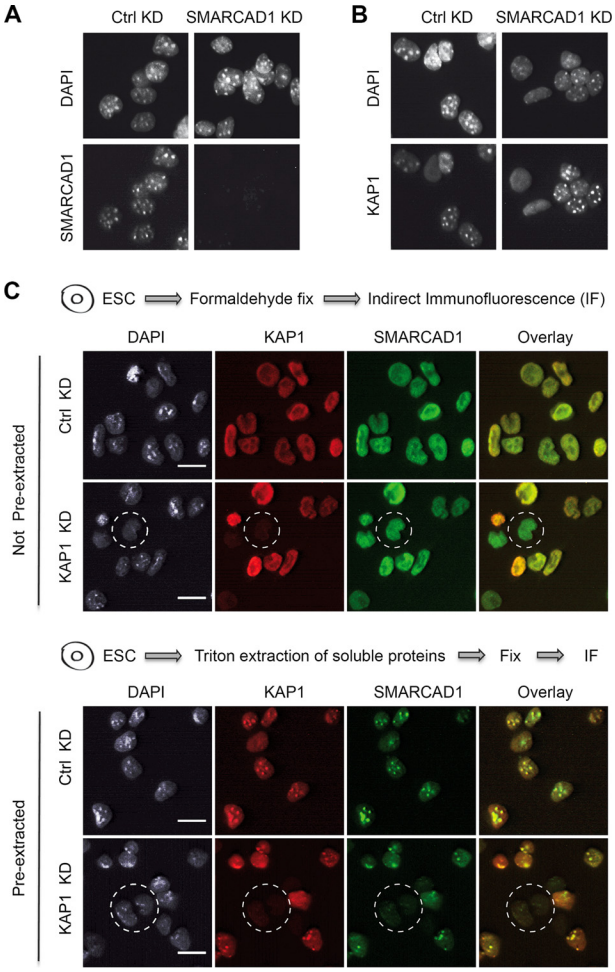

Figure 4. SMARCAD1 protein becomes readily extractable upon KAP1 depletion in ESCs. Representative examples of indirect immunofluorescence for KAP1 and SMARCAD1 proteins upon shRNA-mediated knockdown of either SMARCAD1 or KAP1. *A and B*, stable control knockdown (*Ctrl*) and SMARCAD1 knockdown (*KD*) mouse E14 ESCs were permeabilized, and soluble proteins were extracted before fixation. *A*, clear knockdown of SMARCAD1. *B*, KAP1 localization is not affected when SMARCAD1 is depleted. Similar results were obtained when the experiment was repeated in a different ESC line. DNA was counterstained with DAPI. *C*, KAP1 depletion alters SMARCAD1 binding in the nucleus. Double-staining in PGK12.1 ESCs transfected for 4 days with control or *Kap1* shRNA plasmids without antibiotic selection. Conditions chosen allow detection of untransfected and transfected cells in parallel. Two fixation and permeabilization protocols were used. *Top*, cells were formaldehyde-fixed before permeabilization (not pre-extracted). *Bottom*, extraction of soluble proteins before fixation (pre-extracted). *Dotted circle*, example of SMARCAD1 localization in nuclei depleted for KAP1. *Scale bar*, 10 μm.

knockdown (Fig. 3*A* and Fig. S3, *right-hand panels*), albeit to a lesser extent than the protein levels. Taken together, these results indicate that KAP1 plays a role in the regulation of SMARCAD1 steady-state levels by yet unknown mechanisms.

Conversely, no change in KAP1 RNA or protein levels was observed when we depleted SMARCAD1 either stably (Fig. 3*B*) or acutely with shRNA (Fig. 5*A*) or esiRNAs (Fig. S6*A*).

KAP1 facilitates nuclear retention of SMARCAD1

Classically, histones and non-histone chromosomal proteins were characterized by their different extractability from cells and nuclei. We therefore examined the interdependence of KAP1 and SMARCAD1 at the individual cell level by different extraction methods and indirect immunofluorescence. Both proteins co-localize throughout the ESC nucleus and accumulate at DAPI-dense pericentric heterochromatin in a similar proportion of cells (Fig. 4). Knockdown of SMARCAD1 had no apparent effect on the KAP1 localization pattern in the ESC nucleus (Fig. 4, *A* and *B*). Reciprocally, we analyzed KAP1-depleted cells and KAP1-expressing cells in parallel and performed double-staining of SMARCAD1 and KAP1 (Fig. 4*C*).

We found that depletion of KAP1 alters SMARCAD1 binding in the nucleus (Fig. 4*C*, *dotted circle*). SMARCAD1 could be detected when KAP1 knockdown cells were fixed before permeabilization and antibody staining (Fig. 4*C*, *Not Pre-extracted*). In contrast, in KAP1-depleted cells, SMARCAD1 was largely washed out by pre-extraction of soluble proteins compared with cells that express KAP1 (Fig. 4*C*, *Pre-extracted*). The release of SMARCAD1 from the nucleus by detergent extraction indicates that it is normally stably associated with nuclear components, but this association is dependent on KAP1. We obtained identical results in different ECSs treated with

shRNAs or esiRNAs against *Kap1* and detecting SMARCAD1 with a different antibody (data not shown). That SMARCAD1 can be readily detected in formaldehyde-fixed KAP1 knockdown ESCs by immunofluorescence when protein levels appear reduced by Western blotting is probably due to the differential sensitivity of these assays. These extraction experiments demonstrate that KAP1 is necessary to stably retain SMARCAD1 in the nucleus of mouse ESCs.

Because a relaxed chromatin architecture with a hyperdynamic chromatin protein population is a distinctive feature of pluripotency (1, 7), this ready release of SMARCAD1 could be a property specific to ESCs. To establish the generality of our observation, we turned to human cells. We performed double-staining in HeLa cells depleted for KAP1 (Fig. S4). As in ESCs, when soluble proteins were pre-extracted before fixation, SMARCAD1 staining was lost in HeLa nuclei that lack KAP1.

SMARCAD1 nuclear retention requires an intact CUE1 domain

KAP1 is thus required for stable maintenance of SMARCAD1 in nuclei of both undifferentiated mouse and differentiated human cells. Given the stable interaction of these proteins *in vitro*, a direct mechanism is likely. In this scenario, specific disruption of the KAP1-SMARCAD1 interaction would have consequences similar to those of the complete removal of KAP1. To test this, we investigated whether the SMARCAD1 CUE1 domain mutant, which abolishes KAP1 binding *in vitro*, directly affects the retention of this remodeler in the nucleus and ultimately bound to the genome. Epitope-tagged wildtype and CUE1 F169K/L196K SMARCAD1 constructs were introduced into ESCs carrying a doxycycline-inducible shRNA targeting the 3′-UTR of *Smarcad1*. After treatment with doxycycline, the levels of endogenous SMARCAD1 were diminished (Fig. 5*A*, compare *lanes 1* and 2), whereas exogenous SMARCAD1 was successfully expressed (Fig. 5*A*, *V5*). Importantly, exchanging two hydrophobic amino acids in the CUE1 domain (*mt*) does not affect the expression, stability, or nuclear localization of SMARCAD1, as determined by Western blotting and indirect immunofluorescence using an antibody that recognizes the C-terminal V5 tag (Fig. 5, *A* and *C*). Nor does it affect the stability or localization of KAP1 (Fig. 5, *A* and *C*) or the cell cycle profile (Fig. S5). Next, we wanted to establish that the CUE1 mutation disrupts the interaction with KAP1 *in vivo*. We confirmed that the triple FLAG/V5-tagged SMARCAD1 protein correctly assembled into KAP1 protein complexes by immunoprecipitating the WT from cell extracts and examining the amount of co-precipitated KAP1 (Fig. 5*B*, *lanes 1–3*). Western blot analyses indicated that equivalent amounts of wildtype and mutant FLAG-SMARCAD1 were recovered in immunoprecipitations (Fig. 5*B*, *FLAG*, compare *lane 3* with *lane 6*). However, the association of KAP1 with the mutant SMARCAD1 protein was severely reduced compared with the wildtype protein (Fig. 5*B*, KAP1, compare *lane 3* with *lane 6*). Thus, an intact CUE1 domain is important for the efficient interaction of SMARCAD1 with KAP1 in cells. To further strengthen this observation, we performed indirect immunofluorescence. In double labeling experiments, exogenous SMARCAD1 protein was detected using an antibody that recognizes the C-terminal V5 tag (Fig. 5*C*). Tagged wildtype SMARCAD1 showed co-localization with KAP1 under all conditions tested. Cells expressing SMARCAD1 protein mutated in the CUE1 domain displayed different staining patterns, depending upon whether cells were immediately fixed or soluble proteins were removed by detergent treatment before fixation. SMARCAD1 carrying a CUE1 mutation was readily washed out from cells if they were not fixed before extraction (Fig. 5*C*, *Pre-extracted*). This demonstrates that tethering of SMARCAD1 in the nucleus requires an intact CUE1 domain.

SMARCAD1 CUE1 domain facilitates its binding to KAP1 target genes

Having established that the physical interaction between SMARCAD1 and KAP1 is essential for the retention of SMARCAD1 in the nucleus, we set out to determine whether SMARCAD1 binds to KAP1 target genes in the ESC genome. To this end, we conducted ChIP in ESCs expressing FLAG-tagged wildtype SMARCAD1 protein using a FLAG antibody. In addition, ChIP was performed in untransfected ESCs using antibodies against endogenous SMARCAD1. We selected known KAP1-binding sites in the ESC genome from a published ChIP-seq data set and previous studies for investigation by qPCR (see Fig. 7) (42, 43). The genes chosen represent different categories of KAP1-binding sites, including imprinted control regions (*Peg13*; *Peg3*), promoters (*Fkbp6*), introns (*Pank4*), and 3′-coding exons (*ZNF* genes, *Ezr*). First, we determined whether SMARCAD1 binds to all or a subset of these KAP1 target sites. A link between SMARCAD1 and KAP1 occupancy has not previously been reported in any cell type. Here, we identified all nine loci tested as direct targets of endogenous SMARCAD1 (Fig. 6, *Ctrl*) as well as of FLAG-tagged wildtype SMARCAD1 (Fig. 7, *left panels*, *Ctrl*). SMARCAD1-depleted cells exhibited reduced levels of SMARCAD1 occupancy (Fig. 6, *KD*; Fig. 7 (*left*), *KD*), whereas levels of H3 were unchanged (Fig. S6*B*), confirming the specificity of the assay. An intergenic control region was not enriched in SMARCAD1 (Fig. 7, *bottom*). This establishes for the first time that SMARCAD1 occupies main categories of KAP1 target genes in the ESC genome.

Next we sought to determine whether the SMARCAD1 CUE1 mutation that disrupts its interaction with KAP1 would affect the ability of SMARCAD1 to bind to KAP1 target genes. We carried out FLAG-ChIP in ES cells expressing tagged SMARCAD1 protein, either WT or a CUE1 mutant, and found that SMARCAD1 occupancy at the selected KAP1 target genes is significantly reduced in the CUE1 mutant (Fig. 7*A*, *right*). This is a specific reduction, not observed in immunoprecipitation with the H3 antibody (Fig. 7*B*). Hence, an intact CUE1 domain is required for efficient binding of SMARCAD1 to these genomic sites. Collectively, our results suggest a model whereby SMARCAD1 localization to different categories of KAP1 target genes is dependent on KAP1.

Discussion

In this work, we provide mechanistic insights into the regulation of the ATP-dependent chromatin remodeler SMARCAD1.

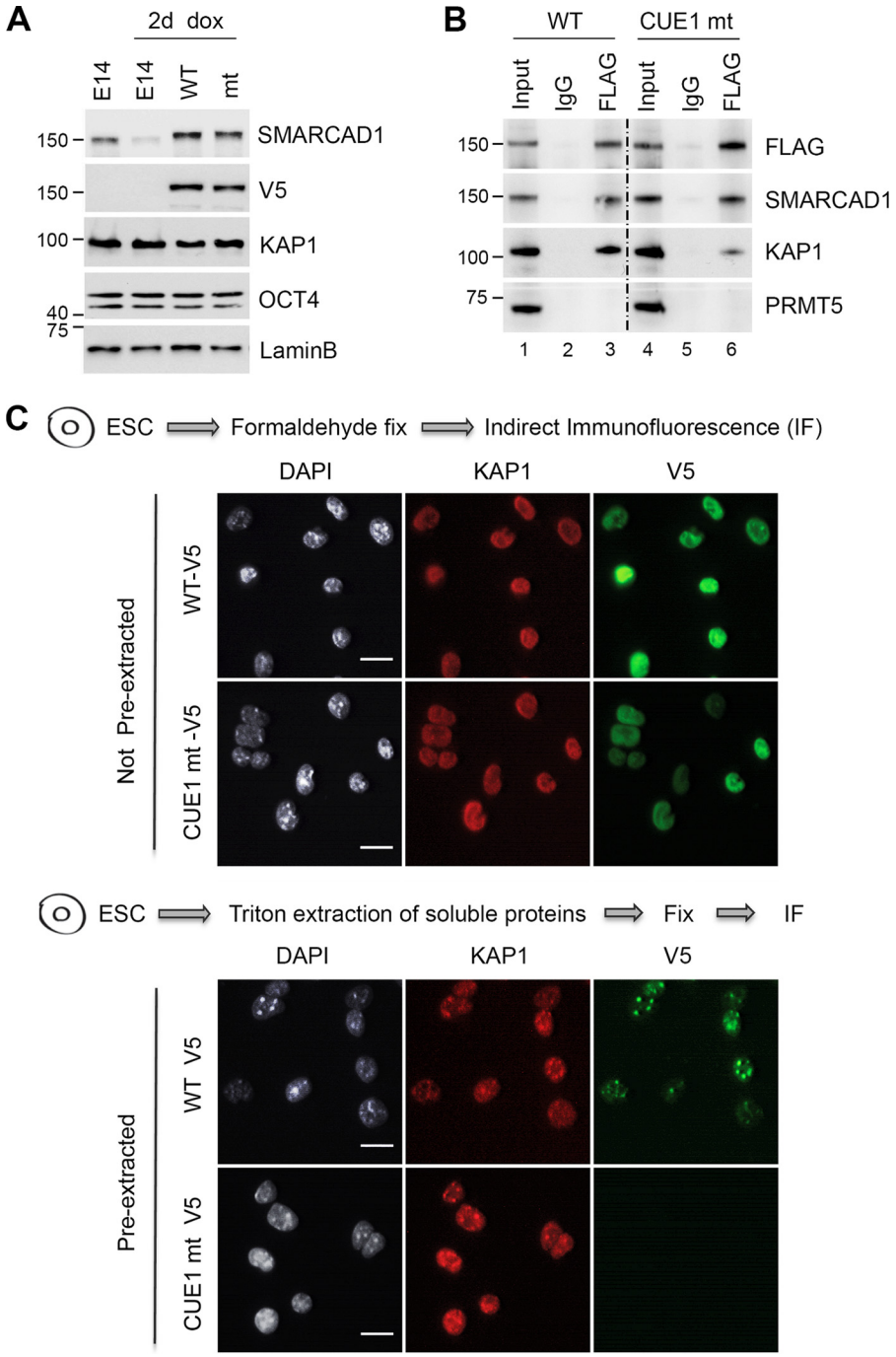

Figure 5. The CUE1 domain in SMARCAD1 is important for its interaction with KAP1 *in vivo*. *A*, characterization of E14 cells expressing tagged SMARCAD1 constructs. An inducible SMARCAD1 knockdown ESC line (*lane 1*) shows effective depletion of SMARCAD1 upon 2 days of treatment with doxycycline (*dox*; *lane 2*). The same cell line was stably transfected with FLAG-*Smarcad1*-V5 constructs, either wildtype (*WT*, *lane 3*) or the CUE1 domain mutant F169K, L196K (*mt*, *lane 4*). To avoid possible artifacts that can arise when comparing single cell clones, we chose to work with pools of transfectants. Tagged WT and mutant proteins are expressed to similar levels. KAP1 and pluripotency marker OCT4 levels are not affected by depletion or overexpression of SMARCAD1. Lamin B1 serves as a loading control. *B*, a FLAG-specific antibody readily co-immunoprecipitates KAP1 from ESCs expressing FLAG-tagged SMARCAD1 WT protein (*lane 3*). The addition of ethidium bromide and Benzonase demonstrated that the interaction of SMARCAD1 and KAP1 is DNA-independent. KAP1 association with FLAG SMARCAD1 is significantly reduced when the CUE1 domain is mutated at F169K and L196K (*lane 6*). *Lanes 1* and *4*, 3% input; *lanes 2* and *5*, IgG. PRMT5 served as a negative control. *Dotted line*, discontinuous lanes from the same gel. Shown is a co-immunoprecipitation performed under conditions where endogenous SMARCAD1 protein was depleted by 2-day doxycycline treatment. Similar results were observed in independent experiments when SMARCAD1 WT and CUE1 mutant constructs were transiently transfected in ESCs expressing endogenous SMARCAD1. *C*, SMARCAD1 remodeler harboring the F169K/L196K mutation in the CUE1 domain is readily extractable from ESC nuclei. Co-staining of KAP1 and V5-tagged SMARCAD1 in E14 cells expressing the CUE1 mutant (*CUE1 mt V5*). ESCs with V5-tagged WT protein served as control (*WT-V5*). Cells were either stained directly or after extraction of soluble proteins. Similar results were obtained in the presence (not shown) or absence of doxycycline (shown). *Scale bar*, 10 μm.

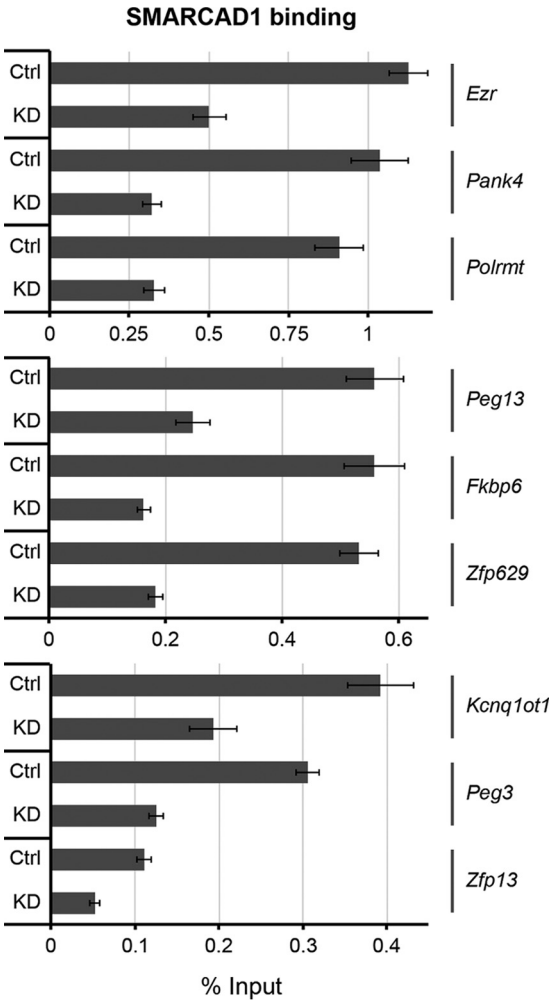

Figure 6. SMARCAD1 binds KAP1 target genes in ESCs. Shown is the measurement of SMARCAD1 occupancy by ChIP-qPCR at KAP1 binding sites in cells that lack exogenous SMARCAD1. After induction of SMARCAD1 knockdown with doxycycline for 2 days (see Fig. 5*A*, *lanes 1* and *2*), a reduction of SMARCAD1 enrichment was apparent at all KAP1 target genes examined (*KD*). One representative experiment of either three (for *Ezr* and *Fkbp6*) or two biological replicates is shown. Percentages of input values are the mean ± S.E. (*error bars*) of three technical replicates.

A key finding is that KAP1 is a major functional co-factor of SMARCAD1 in mouse ESCs. Our results lead us to propose a model whereby the interaction with KAP1 is required for efficient nuclear retention and tethering of SMARCAD1 to genomic binding sites. In direct support for this, we have shown that SMARCAD1 occupies KAP1 target genes in the ESC genome, and this association is disrupted when SMARCAD1 cannot bind KAP1.

SMARCAD1 and KAP1 are expressed throughout development, and both display particularly high levels in ESCs, where they are required to maintain the ESC state (3, 9, 10, 26–28, 40, 41, 44, 46). Our biochemical experiments identify KAP1 as a core component of SMARCAD1 complexes in pluripotent cells. Association between these proteins has been described previously in HeLa, Hct116, and HEK293 cells (13, 30). We have therefore established that this interaction is conserved and has important functions beyond transformed human cells. KAP1 and SMARCAD1 interact directly with each other via their RBCC and CUE1 domains, respectively. They behave similarly in biochemical fractionation experiments and co-localize throughout the ESC nucleoplasm as well as in DAPI-dense staining heterochromatin. This suggests a model in which SMARCAD1-KAP1 complexes operate in both eu- and heterochromatin contexts. Accordingly, KAP1 facilitates the retention of the majority of SMARCAD1 protein in the nucleus in both mouse ESCs and human somatic cells. We therefore consider the physical interaction between SMARCAD1 and KAP1 to be the primary means for tethering SMARCAD1 in the genome. These findings do not exclude the possibility that there are sites in the genome that are bound by SMARCAD1 independently of KAP1. For example, additional mechanisms could involve histone modifications; one potential candidate is citrullinated histone H3 Arg-26, which SMARCAD1 interacts with in ESCs (10).

Steady-state levels of SMARCAD1 are dependent on KAP1 in ESCs. Depletion of KAP1 leads to progressive loss of SMARCAD1. Although the precise mechanisms underlying this are not clear, it implies that previous studies on the effect of KAP1 depletion in ESCs may have not considered the contribution of SMARCAD1. KAP1 function has many facets, including destabilization of heterochromatin at DNA damage sites, stabilizing polymerase II pausing thereby controlling transcriptional elongation, and heterochromatin establishment to silence genes and retrotransposons (34, 35). One proposed function for KAP1 is to protect imprinted genes against the wave of DNA demethylation that affects the mammalian genome during early embryogenesis (43). It remains to be determined whether these or other processes are affected by the SMARCAD1-KAP1 partnership in pluripotent cells. Our ChIP experiments provide the first data consistent with a contribution of SMARCAD1 to KAP1-mediated heterochromatin establishment/maintenance. We observe binding of SMARCAD1 to sites in the ESC genome where KAP1 was previously shown to maintain H3K9me3 and DNA methylation, such as *Fkbp6*, *Zfp629*, and the imprinted control regions of *Peg3* and *Peg13* (43). Thus, SMARCAD1 may be part of the complex comprising KAP1 and chromatin modifiers that preserves the histone modification and DNA methylation status during early embryogenesis. We also identified 3′ exons of zinc finger genes as SMARCAD1 targets. These are generally considered strong KAP1-binding sites and contain repeated DNA sequences encoding zinc finger motifs, 19 in *Zfp629* and 8 in *Zfp13*. It has been proposed that heterochromatinization of ZNF 3′-coding exons may prevent inappropriate recombination between these regions (35). It is achieved by KAP1 acting as a scaffold for the assembly of silencing factors such as the H3K9 methyltransferase SETDB1 and the heterochromatin protein 1 (HP1). *Polrmt* and *Pank4* represent examples of genes marked by KAP1 and H3K9me3 that we find to be co-occupied by SMARCAD1 (42, 48, 49). A SMARCAD1 CUE1 mutant protein displayed reduced binding to all KAP1 targets analyzed, highlighting a critical role for this motif in either the initial targeting of SMARCAD1 to KAP1 target genes or in the stability of the chromatin-bound complex.

We speculate that the importance of the CUE1 motif in facilitating stable localization of SMARCAD1 in the genome is not limited to those selected sites, given that in immunofluores-

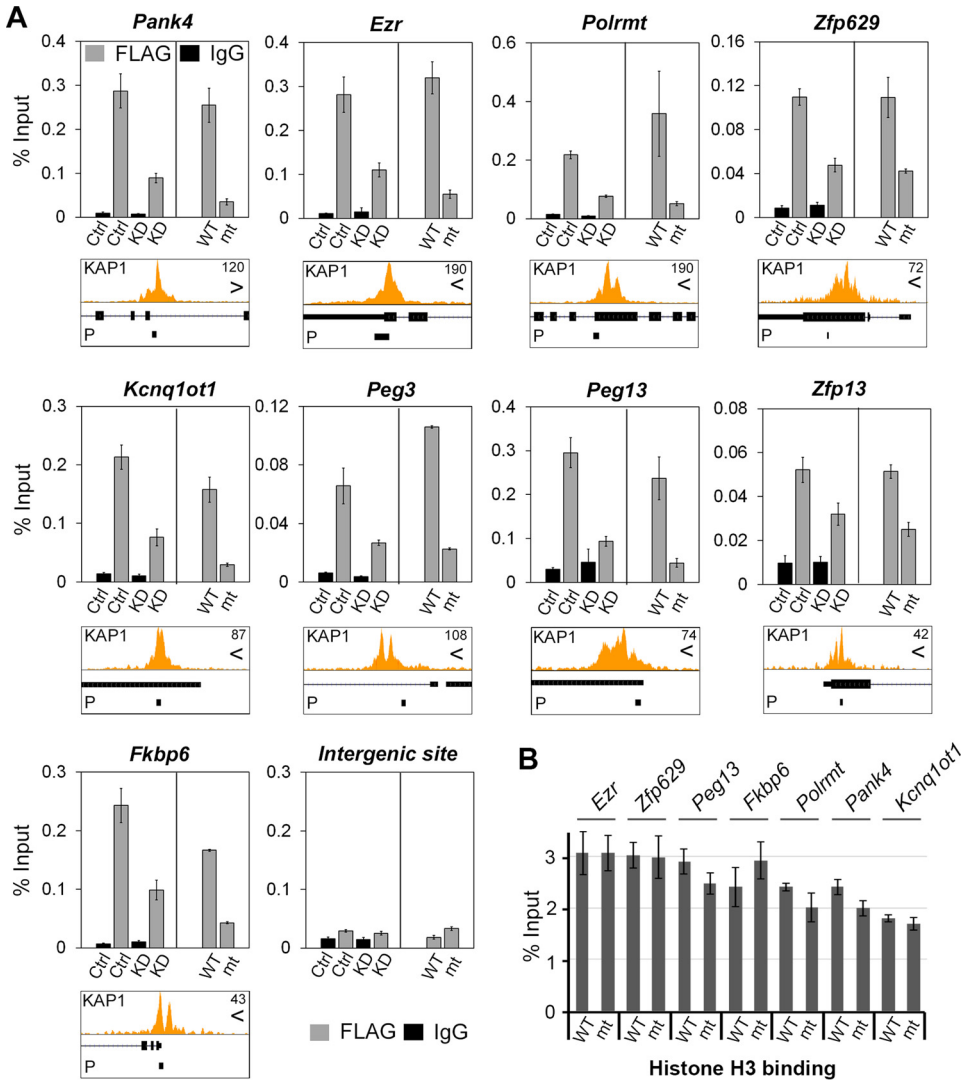

Figure 7. Association of SMARCAD1 with KAP1 target genes depends on the CUE1 domain. *A*, FLAG ChIP followed by real-time PCR analysis to assess FLAG-SMARCAD1 enrichment at KAP1 target genes, including imprinted genes and zinc finger protein (*ZFP*) genes. Screenshots show KAP1 peaks called from the data set of (42). The scale varies between 2.3 and 6.9 kb. The direction of genes and the primers used to detect binding are indicated with an *arrowhead* and a *P*, respectively. Depicted are qPCR data collected for each gene upon SMARCAD1 depletion (*left*) or of SMARCAD1 mutation in the CUE1 domain (*right*). *Left*, E14 ESCs expressing tagged wildtype SMARCAD1 after 2 days of FLUC (*Ctrl*) or *Smarcad1* esiRNA treatment (*KD*); the latter conditions ensure that both endogenous and tagged SMARCAD1 protein levels are diminished (Fig. S6*A*). IgG control is shown, and H3 control is shown in Fig. S6*B*. *Right*, stable SMARCAD1 association with genes bound by KAP1 requires an intact CUE1 domain. Inducible SMARCAD1 knockdown ESCs expressing FLAG SMARCAD1 wildtype (*WT*) or CUE1 mutant protein (*mt*, F169K/L196K) were treated with doxycycline for 2 days to deplete endogenous SMARCAD1. ChIP results represent the mean ± S.E. of biological duplicate experiments. *B*, binding patterns of H3 on KAP1 target genes in E14 ESCs expressing tagged SMARCAD1. Chromatin analyzed corresponds to samples from Fig. 7. *Right*, FLAG WT SMARCAD1 (*WT*) and FLAG SMARCAD1 CUE1 domain mutant F169K/L196K (*mt*).

cence, the vast majority of SMARCAD1 is readily extracted from the nucleus if it carries a CUE1 mutation.

CUE motifs can bind mono- and polyubiquitin and are found in many eukaryotic proteins with various, often cytoplasmic functions, but are not common in ATP-dependent chromatin remodelers (18, 37, 50–52). A possible role for the CUE motifs in SMARCAD1 and its yeast homologs in recognizing ubiquitylated histones has previously been debated. In support, an increase of ubiquitylated H2B was observed in Fun30 target genes, and SMARCAD1 was shown to bind H2A-ubiquitin dependent on intact CUE1 and CUE2 domains (19, 53). However, *in vitro* binding experiments could not detect a preference of Fun30 or SMARCAD1 for ubiquitylated histones compared with unmodified H2 (24, 54). Our *in vitro* binding studies were carried out with recombinant KAP1 protein that was not ubiquitylated, suggesting that the KAP1 SMARCAD1-CUE1 interaction can occur independently of ubiquitin. It remains possible that (i) ubiquitin affects the affinity of this interaction *in vivo*, (ii) a ubiquitin-like mimic within KAP1 mediates the interaction, or, alternatively, (iii) that the CUE1 domain of SMARCAD1 recognizes a motif not related to ubiquitin. A putative homology with ubiquitin in KAP1 was not apparent using standard *in silico* prediction programs. Nor did we detect competition in KAP1-CUE1 binding experiments upon the addition of an excess of pure ubiquitin. Therefore, we postulate the possible existence of a novel, atypical interaction mode of the CUE1 domain of SMARCAD1 with KAP1.

Experimental procedures

Cell lines and plasmids

Mouse ES cells (PGK12.1; J1; E14 and derivatives thereof) were grown on gelatin-coated dishes without feeders in Dulbecco's modified Eagle's medium (Life Technologies, Inc.) supplemented with 15% FBS, 0.1 mM 2-mercaptoethanol, 0.1 mM non-essential amino acids, 2 mM L-glutamine supplemented with leukemia inhibitory factor (1000 units/ml) (Cell Guidance System). Medium with doxycycline (0.5 μg/ml final concentration) was prepared fresh and changed during induction. HeLa cells and KAP1 knockdown clones thereof were described (13). Cell lines tested negative for mycoplasma contamination.

Generation of cell lines for affinity purification—The coding sequence of SMARCAD1 was amplified from mouse ESC cDNA and inserted into a CAG-driven expression vector, with an N-terminal single FLAG tag. Tagged Smarcad1 construct along with the empty vector control were transfected into PGK12.1 ESCs using Lipofectamine 2000 (Invitrogen), and clonal lines were selected with 1.7 μg/ml puromycin. Expression of the tagged SMARCAD1 in selected clones was analyzed by indirect immunofluorescence and Western blot analysis with a FLAG antibody.

Generation of FLAG-SMARCAD1 ES cell lines for ChIP—Wildtype *Smarcad1* and CUE1 double mutant (F169K/L196K) were inserted into a pCAG-driven expression vector with an N-terminal triple FLAG tag and a C-terminal V5 tag. These plasmids were stably integrated into E14 ESCs carrying a doxycycline-inducible shRNA targeting the 3′-UTR of *Smarcad1* as described below before knocking down endogenous SMARCAD1. Cells with stable integrants were selected using 1 μg/ml puromycin. Pools of transfectants were characterized by Western blotting and indirect immunofluorescence.

Knockdown (KD) experiments by RNAi

SMARCAD1 and KAP1 depletion was accomplished with esiRNAs and shRNA vectors using non-targeting controls in parallel. Knockdown efficiency was determined by Western blotting. Synthetic esiRNAs used to achieve transient depletion of SMARCAD1 and KAP1 were from Sigma, MISSION® esiRNA targeting mouse Smarcad1 EMU209081 and mouse Kap1 EMU024081. As a non-targeting control, we used esiRNA against FLUC (Sigma, MISSION® esiRNA EHUFLUC) as described in the manufacturer's instructions. For ChIP experiments, 2×10^7 E14 ESCs were transfected in suspension with 39 μg of esiRNA using Lipofectamine 2000 and analyzed 48 h later. For protein stability analysis, 1×10^6 J1 ESCs were transfected as above with 800 ng of esiRNA twice, on day 0 and day 1, and analyzed 72 h after the first transfection.

Transient depletion of KAP1 was also accomplished with pLKO.1 vectors containing a short hairpin RNA against either *Kap1* (5′-CCGCATGTTCAAACAGTTCAACTCGAGTTGAACTGTTTGAACATGCGG-3′) or a control (5′-CCTAAGGTTAAGTCGCCCTCGCTCGAGCGAGGGCGACTTAACCTTAGG-3′). Puromycin selection (1.2 μg/ml) was started 24 h after transfection of E14 cells with Lipofectamine 2000, and cells were analyzed 3, 4, and 5 days post-transfection.

An shRNA targeting the 3′-UTR of *Smarcad1* was selected from the predictions in Fellmann *et al.* (55) and used in both constitutive and inducible KD experiments. An shRNA targeting *Renilla* luciferase served as a control (56). The constitutive KD vector has eGFP-miRE shRNA backbone and a puromycin resistance driven by a CAG promoter (CAG-eGFP-miRE-IRES-Puro). For the inducible KD, the shRNA eGFP-miRE cassette was cloned into the doxycycline-inducible vector pINDUCER (57). Several features of the original pINDUCER were modified, including changing the constitutive promoter to a CAG promoter and upgrading the inducible promoter to TRE3G. Stable clones of the inducible KD cells were generated by transducing ES cells before inducing knockdown by treatment with 0.5 μg/ml doxycycline. *Smarcad1* shRNA oligo sequence used: 5′-TGCTGTTGACAGTGAGCGACAGCAGAACAGATTAACTTAATAGTGAAGCCACAGATGTATTAAGTTAATCTGTTCTGCTGGTGCCTACTGCCTCGGA-3′.

Purification of FLAG-SMARCAD1 and mass spectrometry

SMARCAD1 was purified from nuclear extracts of PGK12.1 ESCs expressing 1× FLAG-tagged mouse SMARCAD1 protein. Nuclear extract preparations from cells transfected with an empty vector lacking FLAG-SMARCAD1 were used as a negative control. Immunoprecipitation from nuclear extracts using the mouse M2 FLAG antibody (Sigma) was performed for 3 h or overnight (4 °C) in the presence of 150 units/ml Benzonase (Novagen) essentially as described (13, 58). Affinity resin was loaded on spin columns (Thermo Scientific Pierce) and washed twice in 20 mM HEPES, pH 7.6, 100 mM KCl, 0.2 mM EDTA, 1.5 mM $MgCl_2$, 0.5 mM DTT, 20% glycerol, 0.02% Nonidet P-40 and then washed three times in the same buffer without Nonidet P-40. Bound proteins were eluted in the final wash buffer supplemented with 0.3 mg/ml 1× FLAG peptide (Sigma). Eluted proteins were run on polyacrylamide gels, gel slices were trypsinized, and peptides were analyzed by mass spectrometry, as described (58).

Co-immunoprecipitation

Precleared extracts, either 150 μg of nuclear extract or 300 μg of whole cell extract, were incubated with 3–3.5 μg of specific antibody or IgG. 150 units/ml Benzonase (Novagen) and 0.1 μg/μl EtBr were added throughout the procedure to reduce interactions mediated by nucleic acid. Immune complexes were captured by Protein G Dynabeads (Novex). Dynabeads-Ab-Ag complexes were washed four times in 20 mM HEPES, pH 7.6, 100 mM KCl, 0.2 mM EDTA, 1.5 mM MgCl, 0.5 mM DTT, 20% glycerol, 0.05% Triton X-100 containing protease inhibitors and then once in the same buffer but with additional 50 mM NaCl. Immune complexes were eluted with SDS sample buffer.

Immunofluorescence and microscopy

Cultured cells wells dropped onto charged, and in the case of ESCs gelatin-coated, glass slides before fixation with formaldehyde (4% for SMARCAD1, FLAG, and V5; 2% for KAP1) for 5 min (FLAG), 10 min (SMARCAD1, KAP1), or 15 min (V5). Permeabilization was carried out for 10–15 min in PBS/Triton X-100, namely 0.1% for SMARCAD1, 0.2% for V5, and 0.4% for

FLAG and KAP1. Primary antibodies recognized the FLAG tag (Sigma F1804, 1:250), V5 tag (Thermo Scientific R960-25, 1:400), SMARCAD1 anti-CUE domain (13) (1:300), SMARCAD1 (Sigma HPA016737, 1:100), and KAP1 (Abcam ab22553, 1:300; ab10483, 1:50). Secondary antibodies used were Alexa 488 and 594 (Thermo Scientific; 1:500). Counterstaining of nuclei was achieved with DAPI-containing mounting medium (Vector Laboratories, H-1200). Where indicated, immunofluorescence was performed after extraction with detergent and salt to remove soluble proteins. ESCs were extracted with 0.5% Triton X-100 in CSK buffer (10 mM PIPES, pH 6.8, 300 mM sucrose, 100 mM NaCl, 3 mM $MgCl_2$) for 35 s (ESCs) or 60 s (HeLa cells) on ice in the presence of 0.5 mM PMSF and then washed in ice-cold PBS and fixed for 10 min with 4% formaldehyde (Sigma 47608).

Images were acquired on a LEICA DMR fluorescent microscope and processed using Adobe Photoshop CS3 or FIJI. In experiments where different cell lines were compared, these were grown on the same chamber slide and stained and processed simultaneously. Images were collected with the same exposure time, and identical post-processing was used.

Chromatin immunoprecipitation

ChIP assays were performed using a one-day ChIP kit (Diagenode C01010080) and double-cross-linking. About 5×10^7 E14 ES cells/15-cm plate were cross-linked with 2 mM disuccinimidyl glutarate (Thermo Scientific, 20593) in PBS for 45 min at room temperature, washed three times with PBS, and cross-linked with 1% formaldehyde in PBS (Polysciences, 04018) for 10 min at room temperature. Formaldehyde was quenched using 125 mM glycine. After cell lysis, chromatin fragmentation was performed using a Diagenode Bioruptor (20–25 cycles of 30 s on/off) to produce fragments of ~200–600 bp. Immunoprecipitation was performed following the manufacturer's instructions using 100 μg of chromatin and 3 μg of specific antibody (SMARCAD1 HPA016737, Sigma; IgG C15410206, Diagenode; IgG 5381, Sigma; FLAG F1804, Sigma; H3 ab1791, Abcam). Pulldowns using IgGs were used as a negative control. ChIP-enriched DNA was analyzed in triplicate using real-time PCR with SYBR Green (Bio-Rad) on a CFX96 Connect (Bio-Rad) or Agilent MX3000P system. Enrichment values for specific factors were normalized to input. Primer sets used for qPCR are available in Table S1.

Extract preparations, cell fractionations, and Western blot analysis

Nuclear Extracts were prepared according to Dignam *et al.* (59). Total whole-cell extracts were prepared as described previously (60).

Cell fractionations were based on the method presented by Zhang *et al.* (47). ES cell lines stably expressing epitope-tagged SMARCAD1 were treated for 2 days with doxycycline to reduce endogenous SMARCAD1 levels. Asynchronously growing ESCs were trypsinized and washed in ice-cold PBS supplemented with 1 mM benzamidine and 0.5 mM PMSF. The cell pellets were resuspended in 1× packed cell volume (PCV) of CSK buffer (10 mM PIPES, pH 6.8, 300 mM sucrose, 100 mM NaCl, 3 mM $MgCl_2$, 1 mM benzamidine, 0.5 mM PMSF) with 0.1% Triton X-100 and incubated on ice for 3 min. Ten percent of the extract was retained as the "total fraction" and diluted in an equal amount of CSK buffer supplemented with 300 units/ml Benzonase (Novagen), and after 10 min on ice, 5 mM EDTA was added to stop the reaction. The remaining 90% of the lysate was centrifuged at 12,000 rpm for 5 min at 4 °C. The supernatant was retained as the "soluble fraction." The pellet was washed once briefly with 1× PCV CSK buffer and then taken up in 1× PCV CSK buffer supplemented with 300 units/ml Benzonase. After 10 min on ice, 5 mM EDTA was added to stop the reaction. Extract amounts corresponding to the equal numbers of starting cells were analyzed by SDS-PAGE and immunoblotting.

Western blot analysis was performed following standard procedures. Antibodies used were as follows: anti-FLAG F1804 and F3165 (Sigma); anti-V5 R960-25 (Thermo Fisher Scientific); anti-H3 ab1791 (Abcam); anti-SMARCAD1 HPA016737 (Sigma); anti-SMARCAD1 A301-593A (Bethyl); anti-lamin B1 ab16048 (Abcam); anti-KAP1 ab22553 (Abcam); anti-Nanog A300-397A (Bethyl); anti-OCT4 sc5279 (Santa Cruz Biotechnology, Inc.); anti-GAPDH sc25778 (Santa Cruz Biotechnology); anti-PRMT5 07-405 (Millipore). Visualization of antibodies was carried out using Immobilon™ Western chemiluminescent HRP substrate (Millipore) using X-ray film or ChemiDoc (Bio-Rad). For quantification, Western blots developed with the ChemiDoc imaging system were analyzed using Image Lab software (Bio-Rad) applying the global subtraction method, normalizing SMARCAD1 signal to the loading control lamin B1.

Recombinant proteins

His-tagged human SMARCAD1 and KAP1 baculovirus expression constructs were provided by Dr. P. Varga-Weisz (13). Proteins were prepared from infected Sf9 cells by four freeze-thaw cycles in 250 mM NaCl, 20 mM HEPES, pH 7.5, 10% glycerol, and protease inhibitors. Proteins were bound to a nickel-agarose column (Qiagen 30210). After washing, bound protein was eluted in the same buffer containing 5 mM imidazole. Fractions containing pure protein were dialyzed against the same buffer plus 1 mM 2-mercaptoethanol. V5-tagged human SMARCAD1 was produced from the pCDNA3.1/nV5-DEST hSMARCAD1-wt plasmid (13) *in vitro* in a T7 TNT coupled transcription–translation reaction (Promega).

GST and GST fusion proteins were expressed in *E. coli* BL21DE3 or Rosetta (Novagen) strains and purified using a C3 Liquidiser (Avestin Europe GmbH). Human KAP1 GST constructs were described previously (45). In brief, the GST-KAP1 fusion constructs in pGEX-4T-1 vectors were KAP1 (aa 1–835), RBCC (aa 1–376), HP1 (aa 376–628), and PB (aa 628–835) and ΔPB (aa 1–628) and ΔRBCC (aa 376–835). Full-length human SMARCAD1 (aa 1–1026) and double CUE domain (dCUE aa 131–367) were cloned into pGEX4T1 by Gibson assembly (Gibson Assembly Master Mix NEB E2611). CUE1 (aa 131–203) and CUE2 (aa 246–295) domains were generated by ligating gBlocks (IDT) flanked by BamHI and XhoI sites into the appropriately cleaved pGEX6P1 vectors. Point mutations in the CUE1 domain were generated using the same approach, either P170G or the double mutation F169K/L196K.

GST pulldown assays

Binding experiments with recombinant proteins utilized 25 μl of packed glutathione-Sepharose 4B beads (GE Healthcare) with 10–15 μg of GST or GST fusion protein to give an effective concentration in the micromolar range in the binding reactions. A blocking step was regularly incorporated into the assay in which beads were blocked with 1% fish gelatin and 1 mg/ml BSA in binding buffer at 4 °C for 1 h followed by three washes in binding buffer. Pure recombinant target protein was mixed with GST fusion protein beads to give a final concentration of 0.2–0.5 μM in a final volume of 150 μl and incubated for 1.5 h at 4 °C. Beads were washed three times in binding buffer, and bound proteins were eluted from the beads with two sequential extractions in SDS sample buffer at room temperature. Bound proteins were detected by Western blotting.

His-SMARCAD1 GST-KAP1 binding experiments were performed in BC250 (250 mM NaCl, 10% glycerol, 20 mM HEPES, pH 7.6, 0.1 mM PMSF, 0.1 mM benzamidine) and washed in BC800 (800 mM NaCl, 10% glycerol, 20 mM HEPES, pH 7.6, 0.1 mM PMSF, 0.1 mM benzamidine).

His-KAP1 GST-SMARCAD1 binding reactions and washes were carried out in 100 mM NaCl, 5% glycerol, 20 mM HEPES, pH 7.6, 0.1% Triton, 0.1 mM PMSF, 0.1 mM benzamidine. In competition experiments, pure ubiquitin (Sigma) was added simultaneously with KAP1 at the concentrations shown in Fig. 2.

Binding reactions using GST fusion proteins and target proteins generated in the T7 TNT reaction were carried out in 20 mM HEPES, pH 7.5, 75 mM KCl, 0.1 mM EDTA, 2.5 mM $MgCl_2$, 1 mM DTT, 0.05% Triton X-100 as recommended by the supplier.

Real-time PCR

Total RNA was extracted with TRIzol (Invitrogen), and cDNA was synthesized using SuperScript II reverse transcriptase (Invitrogen) following the supplier's recommendations. qPCRs were performed on the CFX Connect real-time PCR detection system (Bio-Rad) or Agilent MX3000P, using iTaq Universal SYBR Green (Bio-Rad). Pairs of primers were evaluated for generating single-peak melting profiles and for linear amplification over a range of DNA template dilutions. qPCR assays were performed in technical triplicates. Three housekeeping genes (*Gapdh*, *Hsp90ab1*, and *Atp5b*) were used as references for normalization. Primers are listed in Table S1.

Flow cytometry

ESCs resuspended in 200 μl of PBS were fixed by the dropwise addition of 1.3 ml of ice-cold 70% ethanol. After fixation at 4 °C, cells were taken up in PI/RNase staining buffer (BD Pharmingen, 550825), incubated for 15 min at room temperature, and analyzed using a BD LSR II cytometer and FlowJo version 10.2 software.

Author contributions—D.D., P.B., and J.E.M. data curation; D.D., P.B., P.S., and J.E.M. formal analysis; D.D., P.B., and P.S. validation; D.D., P.B., P.S., M.K., T.R., N.B., J.D., M.D., and R.A.P. investigation; D.D. and P.B. visualization; D.D., P.B., P.S., and J.E.M. writing-original draft; J.E.M. conceptualization; J.E.M. supervision; J.E.M. funding acquisition; J.E.M. project administration.

Acknowledgments—We thank Ke Lan (Institut Pasteur of Shanghai, China) and Patrick Varga-Weisz (Babraham Institute, Babraham, UK) for GST and baculovirus constructs and Miguel Branco (Blizard Institute, London, UK) and Xu Han (Life Sciences Institute, Zhejiang University) for pKLO.1 plasmids. We are grateful to Christina Schlagheck for her contribution to the acquisition of data and to Bianca Bamberger and Katrin Treutwein for excellent technical assistance. We thank Lienhardt Schmitz, Colin Dingwall, Guntram Suske, Boris Lamp, and Karim Bouazoune for helpful discussions. We acknowledge the laboratories of Roland Lill and Alexander Brehm (Philipps University of Marburg, Germany) for help with liquidizer and baculovirus expression.

References

1. Lessard, J. A., and Crabtree, G. R. (2010) Chromatin regulatory mechanisms in pluripotency. *Annu. Rev. Cell Dev. Biol.* **26,** 503–532 CrossRef Medline
2. Hota, S. K., and Bruneau, B. G. (2016) ATP-dependent chromatin remodeling during mammalian development. *Development* **143,** 2882–2897 CrossRef Medline
3. Fazzio, T. G., Huff, J. T., and Panning, B. (2008) An RNAi screen of chromatin proteins identifies Tip60-p400 as a regulator of embryonic stem cell identity. *Cell* **134,** 162–174 CrossRef Medline
4. Ho, L., Miller, E. L., Ronan, J. L., Ho, W. Q., Jothi, R., and Crabtree, G. R. (2011) esBAF facilitates pluripotency by conditioning the genome for LIF/STAT3 signalling and by regulating polycomb function. *Nat. Cell Biol.* **13,** 903–913 CrossRef Medline
5. Kidder, B. L., Palmer, S., and Knott, J. G. (2009) SWI/SNF-Brg1 regulates self-renewal and occupies core pluripotency-related genes in embryonic stem cells. *Stem Cells* **27,** 317–328 CrossRef Medline
6. Gaspar-Maia, A., Alajem, A., Polesso, F., Sridharan, R., Mason, M. J., Heidersbach, A., Ramalho-Santos, J., McManus, M. T., Plath, K., Meshorer, E., and Ramalho-Santos, M. (2009) Chd1 regulates open chromatin and pluripotency of embryonic stem cells. *Nature* **460,** 863–868 CrossRef Medline
7. Mattout, A., and Meshorer, E. (2010) Chromatin plasticity and genome organization in pluripotent embryonic stem cells. *Curr. Opin. Cell Biol.* **22,** 334–341 CrossRef Medline
8. Ho, L., and Crabtree, G. R. (2010) Chromatin remodelling during development. *Nature* **463,** 474–484 CrossRef Medline
9. Leeb, M., Dietmann, S., Paramor, M., Niwa, H., and Smith, A. (2014) Genetic Exploration of the exit from self-renewal using haploid embryonic stem cells. *Cell Stem Cell* **14,** 385–393 CrossRef Medline
10. Xiao, S., Lu, J., Sridhar, B., Cao, X., Yu, P., Zhao, T., Chen, C. C., McDee, D., Sloofman, L., Wang, Y., Rivas-Astroza, M., Telugu, B. P. V. L., Levasseur, D., Zhang, K., Liang, H., *et al.* (2017) SMARCAD1 contributes to the regulation of naive pluripotency by interacting with histone citrullination. *Cell Rep.* **18,** 3117–3128 CrossRef Medline
11. Hong, F., Fang, F., He, X., Cao, X., Chipperfield, H., Xie, D., Wong, W. H., Ng, H. H., and Zhong, S. (2009) Dissecting early differentially expressed genes in a mixture of differentiating embryonic stem cells. *PLoS Comput. Biol.* **5,** e1000607 CrossRef Medline
12. Durand-Dubief, M., Will, W. R., Petrini, E., Theodorou, D., Harris, R. R., Crawford, M. R., Paszkiewicz, K., Krueger, F., Correra, R. M., Vetter, A. T., Miller, J. R., Kent, N. A., and Varga-Weisz, P. (2012) SWI/SNF-like chromatin remodeling factor Fun30 supports point centromere function in *S. cerevisiae*. *PLoS Genet.* **8,** e1002974 CrossRef Medline
13. Rowbotham, S. P., Barki, L., Neves-Costa, A., Santos, F., Dean, W., Hawkes, N., Choudhary, P., Will, W. R., Webster, J., Oxley, D., Green, C. M., Varga-Weisz, P., and Mermoud, J. E. (2011) Maintenance of silent chromatin through replication requires SWI/SNF-like chromatin remodeler SMARCAD1. *Mol. Cell* **42,** 285–296 CrossRef Medline
14. Strålfors, A., Walfridsson, J., Bhuiyan, H., and Ekwall, K. (2011) The FUN30 chromatin remodeler, Fft3, protects centromeric and subtelo-

meric domains from euchromatin formation. *PLoS Genet.* **7,** e1001334 CrossRef Medline
15. Steglich, B., Stralfors, A., Khorosjutina, O., Persson, J., Smialowska, A., Javerzat, J. P., and Ekwall, K. (2015) The Fun30 chromatin remodeler Fft3 controls nuclear organization and chromatin structure of insulators and subtelomeres in fission yeast. *PLoS Genet.* **11**
16. Taneja, N., Zofall, M., Balachandran, V., Thillainadesan, G., Sugiyama, T., Wheeler, D., Zhou, M., and Grewal, S. I. (2017) SNF2 family protein Fft3 suppresses nucleosome turnover to promote epigenetic inheritance and proper replication. *Mol. Cell* **66,** 50–62.e6 CrossRef Medline
17. Yu, Q., Zhang, X., and Bi, X. (2011) Roles of chromatin remodeling factors in the formation and maintenance of heterochromatin structure. *J. Biol. Chem.* **286,** 14659–14669 CrossRef Medline
18. Neves-Costa, A., Will, W. R., Vetter, A. T., Miller, J. R., and Varga-Weisz, P. (2009) The SNF2-family member Fun30 promotes gene silencing in heterochromatic loci. *PLoS One* **4,** e8111 CrossRef Medline
19. Byeon, B., Wang, W., Barski, A., Ranallo, R. T., Bao, K., Schones, D. E., Zhao, K., Wu, C., and Wu, W. H. (2013) The ATP-dependent chromatin remodeling enzyme Fun30 represses transcription by sliding promoter-proximal nucleosomes. *J. Biol. Chem.* **288,** 23182–23193 CrossRef Medline
20. Doiguchi, M., Nakagawa, T., Imamura, Y., Yoneda, M., Higashi, M., Kubota, K., Yamashita, S., Asahara, H., Iida, M., Fujii, S., Ikura, T., Liu, Z., Nandu, T., Kraus, W. L., Ueda, H., and Ito, T. (2016) SMARCAD1 is an ATP-dependent stimulator of nucleosomal H2A acetylation via CBP, resulting in transcriptional regulation. *Sci. Rep.* **6,** 20179 CrossRef Medline
21. Lee, J., Choi, E. S., Seo, H. D., Kang, K., Gilmore, J. M., Florens, L., Washburn, M. P., Choe, J., Workman, J. L., and Lee, D. (2017) Chromatin remodeller Fun30Fft3 induces nucleosome disassembly to facilitate RNA polymerase II elongation. *Nat. Commun.* **8,** 14527 CrossRef Medline
22. Rother, M. B., and van Attikum, H. (2017) DNA repair goes hip-hop: SMARCA and CHD chromatin remodellers join the break dance. *Philos. Trans. R. Soc. Lond. B Biol. Sci.* **372,** 20160285 CrossRef Medline
23. Adkins, N. L., Swygert, S. G., Kaur, P., Niu, H., Grigoryev, S. A., Sung, P., Wang, H., and Peterson, C. L. (2017) Nucleosome-like, single-stranded DNA (ssDNA)-histone octamer complexes and the implication for DNA double strand break repair. *J. Biol. Chem.* **292,** 5271–5281 CrossRef Medline
24. Awad, S., Ryan, D., Prochasson, P., Owen-Hughes, T., and Hassan, A. H. (2010) The Snf2 homolog Fun30 acts as a homodimeric ATP-dependent chromatin-remodeling enzyme. *J. Biol. Chem.* **285,** 9477–9484 CrossRef Medline
25. Schoor, M., Schuster-Gossler, K., Roopenian, D., and Gossler, A. (1999) Skeletal dysplasias, growth retardation, reduced postnatal survival, and impaired fertility in mice lacking the SNF2/SWI2 family member ETL1. *Mech. Dev.* **85,** 73–83 CrossRef Medline
26. Loh, Y. H., Wu, Q., Chew, J. L., Vega, V. B., Zhang, W., Chen, X., Bourque, G., George, J., Leong, B., Liu, J., Wong, K. Y., Sung, K. W., Lee, C. W., Zhao, X. D., Chiu, K. P., *et al.* (2006) The Oct4 and Nanog transcription network regulates pluripotency in mouse embryonic stem cells. *Nat. Genet.* **38,** 431–440 CrossRef Medline
27. Efroni, S., Duttagupta, R., Cheng, J., Dehghani, H., Hoeppner, D. J., Dash, C., Bazett-Jones, D. P., Le Grice, S., McKay, R. D., Buetow, K. H., Gingeras, T. R., Misteli, T., and Meshorer, E. (2008) Global transcription in pluripotent embryonic stem cells. *Cell Stem Cell* **2,** 437–447 CrossRef Medline
28. Schoor, M., Schuster-Gossler, K., and Gossler, A. (1993) The Etl-1 gene encodes a nuclear protein differentially expressed during early mouse development. *Dev. Dyn.* **197,** 227–237 CrossRef Medline
29. Yan, Z., Wang, Z., Sharova, L., Sharov, A. A., Ling, C., Piao, Y., Aiba, K., Matoba, R., Wang, W., and Ko, M. S. H. (2008) BAF250B-associated SWI/SNF chromatin-remodeling complex is required to maintain undifferentiated mouse embryonic stem cells. *Stem Cells* **26,** 1155–1165 CrossRef Medline
30. Okazaki, N., Ikeda, S., Ohara, R., Shimada, K., Yanagawa, T., Nagase, T., Ohara, O., and Koga, H. (2008) The novel protein complex with SMARCAD1/KIAA1122 binds to the vicinity of TSS. *J. Mol. Biol.* **382,** 257–265 CrossRef Medline
31. Marcon, E., Jain, H., Bhattacharya, A., Guo, H., Phanse, S., Pu, S., Byram, G., Collins, B. C., Dowdell, E., Fenner, M., Guo, X., Hutchinson, A., Kennedy, J. J., Krastins, B., Larsen, B., *et al.* (2015) Assessment of a method to characterize antibody selectivity and specificity for use in immunoprecipitation. *Nature methods* **12,** 725–731 CrossRef Medline
32. Loyola, A., Tagami, H., Bonaldi, T., Roche, D., Quivy, J. P., Imhof, A., Nakatani, Y., Dent, S. Y., and Almouzni, G. (2009) The HP1α-CAF1-SetDB1-containing complex provides H3K9me1 for Suv39-mediated K9me3 in pericentric heterochromatin. *EMBO Rep.* **10,** 769–775 CrossRef Medline
33. Cheng, B., Ren, X., and Kerppola, T. K. (2014) KAP1 represses differentiation-inducible genes in embryonic stem cells through cooperative binding with PRC1 and derepresses pluripotency-associated genes. *Mol. Cell. Biol.* **34,** 2075–2091 CrossRef Medline
34. Cheng, C. T., Kuo, C. Y., and Ann, D. K. (2014) KAPtain in charge of multiple missions: emerging roles of KAP1. *World J. Biol. Chem.* **5,** 308–320 CrossRef Medline
35. Iyengar, S., and Farnham, P. J. (2011) KAP1 protein: an enigmatic master regulator of the genome. *J. Biol. Chem.* **286,** 26267–26276 CrossRef Medline
36. Ishihama, Y., Oda, Y., Tabata, T., Sato, T., Nagasu, T., Rappsilber, J., and Mann, M. (2005) Exponentially modified protein abundance index (emPAI) for estimation of absolute protein amount in proteomics by the number of sequenced peptides per protein. *Mol. Cell. Proteomics* **4,** 1265–1272 CrossRef Medline
37. Hurley, J. H., Lee, S., and Prag, G. (2006) Ubiquitin-binding domains. *Biochem. J.* **399,** 361–372 CrossRef Medline
38. Boyer, L. A., Lee, T. I., Cole, M. F., Johnstone, S. E., Levine, S. S., Zucker, J. P., Guenther, M. G., Kumar, R. M., Murray, H. L., Jenner, R. G., Gifford, D. K., Melton, D. A., Jaenisch, R., and Young, R. A. (2005) Core transcriptional regulatory circuitry in human embryonic stem cells. *Cell* **122,** 947–956 CrossRef Medline
39. Rowe, H. M., Jakobsson, J., Mesnard, D., Rougemont, J., Reynard, S., Aktas, T., Maillard, P. V., Layard-Liesching, H., Verp, S., Marquis, J., Spitz, F., Constam, D. B., and Trono, D. (2010) KAP1 controls endogenous retroviruses in embryonic stem cells. *Nature* **463,** 237–240 CrossRef Medline
40. Hu, G., Kim, J., Xu, Q., Leng, Y., Orkin, S. H., and Elledge, S. J. (2009) A genome-wide RNAi screen identifies a new transcriptional module required for self-renewal. *Genes Dev.* **23,** 837–848 CrossRef Medline
41. Seki, Y., Kurisaki, A., Watanabe-Susaki, K., Nakajima, Y., Nakanishi, M., Arai, Y., Shiota, K., Sugino, H., and Asashima, M. (2010) TIF1β regulates the pluripotency of embryonic stem cells in a phosphorylation-dependent manner. *Proc. Natl. Acad. Sci. U.S.A.* **107,** 10926–10931 CrossRef Medline
42. Elsässer, S. J., Noh, K. M., Diaz, N., Allis, C. D., and Banaszynski, L. A. (2015) Histone H3.3 is required for endogenous retroviral element silencing in embryonic stem cells. *Nature* **522,** 240–244 CrossRef Medline
43. Quenneville, S., Verde, G., Corsinotti, A., Kapopoulou, A., Jakobsson, J., Offner, S., Baglivo, I., Pedone, P. V., Grimaldi, G., Riccio, A., and Trono, D. (2011) In embryonic stem cells, ZFP57/KAP1 recognize a methylated hexanucleotide to affect chromatin and DNA methylation of imprinting control regions. *Mol. Cell* **44,** 361–372 CrossRef Medline
44. Cammas, F., Mark, M., Dollé, P., Dierich, A., Chambon, P., and Losson, R. (2000) Mice lacking the transcriptional corepressor TIF1β are defective in early postimplantation development. *Development* **127,** 2955–2963 Medline
45. Sun, R., Liang, D., Gao, Y., and Lan, K. (2014) Kaposi's sarcoma-associated herpesvirus-encoded LANA interacts with host KAP1 to facilitate establishment of viral latency. *J. Virol.* **88,** 7331–7344 CrossRef Medline
46. Hong, F., Fang, F., He, X., Cao, X., Chipperfield, H., Xie, D., Wong, W. H., Ng, H. H., and Zhong, S. (2009) Dissecting early differentially expressed genes in a mixture of differentiating embryonic stem cells. *PLoS Comput. Biol.* **5,** e1000607 CrossRef Medline
47. Zhang, Z. M., Rothbart, S. B., Allison, D. F., Cai, Q., Harrison, J. S., Li, L., Wang, Y., Strahl, B. D., Wang, G. G., and Song, J. (2015) An allosteric interaction links USP7 to deubiquitination and chromatin targeting of UHRF1. *Cell Rep.* **12,** 1400–1406 CrossRef Medline

48. Mikkelsen, T. S., Ku, M., Jaffe, D. B., Issac, B., Lieberman, E., Giannoukos, G., Alvarez, P., Brockman, W., Kim, T. K., Koche, R. P., Lee, W., Mendenhall, E., O'Donovan, A., Presser, A., Russ, C., *et al.* (2007) Genome-wide maps of chromatin state in pluripotent and lineage-committed cells. *Nature* **448,** 553–560 CrossRef Medline
49. Strogantsev, R., Krueger, F., Yamazawa, K., Shi, H., Gould, P., Goldman-Roberts, M., McEwen, K., Sun, B., Pedersen, R., and Ferguson-Smith, A. C. (2015) Allele-specific binding of ZFP57 in the epigenetic regulation of imprinted and non-imprinted monoallelic expression. *Genome Biol.* **16,** 112 CrossRef Medline
50. Kang, R. S., Daniels, C. M., Francis, S. A., Shih, S. C., Salerno, W. J., Hicke, L., and Radhakrishnan, I. (2003) Solution structure of a CUE-ubiquitin complex reveals a conserved mode of ubiquitin binding. *Cell* **113,** 621–630 CrossRef Medline
51. Shih, S. C., Prag, G., Francis, S. A., Sutanto, M. A., Hurley, J. H., and Hicke, L. (2003) A ubiquitin-binding motif required for intramolecular monoubiquitylation, the CUE domain. *EMBO J.* **22,** 1273–1281 CrossRef Medline
52. Prag, G., Misra, S., Jones, E. A., Ghirlando, R., Davies, B. A., Horazdovsky, B. F., and Hurley, J. H. (2003) Mechanism of ubiquitin recognition by the CUE domain of Vps9p. *Cell* **113,** 609–620 CrossRef Medline
53. Densham, R. M., Garvin, A. J., Stone, H. R., Strachan, J., Baldock, R. A., Daza-Martin, M., Fletcher, A., Blair-Reid, S., Beesley, J., Johal, B., Pearl, L. H., Neely, R., Keep, N. H., Watts, F. Z., and Morris, J. R. (2016) Human BRCA1-BARD1 ubiquitin ligase activity counteracts chromatin barriers to DNA resection. *Nat. Struct. Mol. Biol.* **23,** 647–655 CrossRef Medline
54. Densham, R. M., and Morris, J. R. (2017) The BRCA1 ubiquitin ligase function sets a new trend for remodelling in DNA repair. *Nucleus* **8,** 116–125 CrossRef Medline
55. Fellmann, C., Hoffmann, T., Sridhar, V., Hopfgartner, B., Muhar, M., Roth, M., Lai, D. Y., Barbosa, I. A. M., Kwon, J. S., Guan, Y., Sinha, N., and Zuber, J. (2013) An optimized microRNA backbone for effective single-copy RNAi. *Cell Rep.* **5,** 1704–1713 CrossRef Medline
56. Fellmann, C., Zuber, J., McJunkin, K., Chang, K., Malone, C. D., Dickins, R. A., Xu, Q., Hengartner, M. O., Elledge, S. J., Hannon, G. J., and Lowe, S. W. (2011) Functional identification of optimized RNAi triggers using a massively parallel sensor assay. *Mol. Cell* **41,** 733–746 CrossRef Medline
57. Meerbrey, K. L., Hu, G., Kessler, J. D., Roarty, K., Li, M. Z., Fang, J. E., Herschkowitz, J. I., Burrows, A. E., Ciccia, A., Sun, T., Schmitt, E. M., Bernardi, R. J., Fu, X., Bland, C. S., Cooper, T. A., Schiff, R., Rosen, J. M., Westbrook, T. F., and Elledge, S. J. (2011) The pINDUCER lentiviral toolkit for inducible RNA interference *in vitro* and *in vivo*. *Proc. Natl. Acad. Sci. U.S.A.* **108,** 3665–3670 CrossRef Medline
58. van den Berg, D. L., Snoek, T., Mullin, N. P., Yates, A., Bezstarosti, K., Demmers, J., Chambers, I., and Poot, R. A. (2010) An Oct4-centered protein interaction network in embryonic stem cells. *Cell Stem Cell* **6,** 369–381 CrossRef Medline
59. Dignam, J. D., Lebovitz, R. M., and Roeder, R. G. (1983) Accurate transcription initiation by RNA polymerase II in a soluble extract from isolated mammalian nuclei. *Nucleic Acids Res.* **11,** 1475–1489 CrossRef Medline
60. Mermoud, J. E., Costanzi, C., Pehrson, J. R., and Brockdorff, N. (1999) Histone macroH2A1.2 relocates to the inactive X chromosome after initiation and propagation of X-inactivation. *J. Cell Biol.* **147,** 1399–1408 CrossRef Medline